Progress In Electromagnetics Research, Vol. 113, 211–226, 2011

NUMERICAL ANALYSIS OF ENHANCED TRANSMISSION THROUGH A SINGLE SUBWAVELENGTH APERTURE BASED ON MIE RESONANCE SINGLE PARTICLE

L. Kang, V. Sadaune, and D. Lippens

Institut d'Electronique de Microélectronique et de Nanotechnologies
UMR CNRS 8520
Université des Sciences et Technlogies de Lille
Avenue Poincaré, BP 60069, Villeneuve d'Ascq Cedex 59652, France

Abstract—We numerically demonstrate that the transmission through a deep subwavelength ($\lambda_0/20$) aperture in a metal plate could be greatly enhanced owing to the resonance effects of a high permittivity (κ) dielectric cube tightly coupled to the aperture. The transmission enhancement originates from the confinement and re-radiation of the electromagnetic energy impinging onto the high κ cube which operates in the 1st Mie resonance mode, and behaves as an ultra-small magnetic dipole antenna. The complex permittivity of the cube governs the operating frequency and the enhancement in terms of bandwidth and transmissivity maximum. Additionally, based on the isotropic response of the high κ cube with dimensions comparable to the aperture size, the almost independence of the enhancement properties on the illumination polarization and incidence angle was assessed.

1. INTRODUCTION

Enhanced transmission of Electro-Magnetic (EM) wave through a single subwavelength aperture (SSA) has been investigated for decades because of both the physics emerging from the simple system and broad application prospects. Considering the quite different conductivity properties of metal (which is generally used to construct the SSA system) at low frequency (e.g., microwave) and in optics, the corresponding enhanced transmission originates from distinct

Received 27 December 2010, Accepted 28 January 2011, Scheduled 2 February 2011
Corresponding author: Didier Lippens (Didier.lippens@iemn.univ-lille1.fr).

mechanisms [1]. Bethe studied the transmission in detail through a SSA in a perfect conductor plate with infinitely thin thickness [2]. These assumptions are sufficient to describe the transmission behavior of EM waves at microwave and radio frequency through a SSA generally in a very thin copper plate. However, both theory [3–9] and experiment [10–13] have verified that Bethe theory is no longer valid in optics and thus at frequencies much higher than the collision one of the metal plate [1]. For instance, developing an analytical model that proves that SSAs behave as magnetic dipoles, Ref. [8] provides a thorough study of light diffraction through a SSA on a real metal and compares the directivity with Bethe and Jackson' theories. The deviation between theories applied at microwave and in optics arises from the transversal and longitudinal surface plasma resonance (SPR) around and within SSAs [1]. For instance, recent investigations of SPR in metallic structures showed enhanced transmission in the visible frequency range through nano-scale SSA fabricated in an Ag film patterned with periodic corrugations on the surface [13]. Implementing a similar concept at microwave frequencies is difficult because SPRs cannot be excited on the surface of common metals which can be considered as perfect conductors in this frequency range [14]. By placing split ring resonator (SRR) at the near field of a SSA in a copper plate, Aydin et al. experimentally demonstrated impressive enhanced transmission around 3.7 GHz, in which no SPR effects was involved [15]. The basic idea in these transmission enhancement studies can be understood as the combination of two effects, i.e., subwavelength localization and re-radiation of the EM energy. The difference is that SPR based enhancement concentrates and re-radiates optical energy by means of excitation and manipulation of surface plasmon polaritons on the structured metal surface [13] while SRR-based devices take advantage of metamaterial unit cell resonance [15, 16].

Recently different groups have verified theoretically and experimentally that ferroelectrics cube arrays which can be considered as High Permittivitty Particle (HPP) behave electromagnetically as negative permeability metamaterials (NPMs) around their 1st Mie resonance frequency (ω_0) [17–22]. One can find a summary of work in a recent review paper [23]. At the 1st Mie resonance mode, as shown in Fig. 1 from the mapping of the displacement currents which exhibit current loop patterns, a single HPP can be regarded as a subwavelength ($\lambda_0/20$ here) magnetic dipole oscillating at the resonant frequency [24]. Furthermore, owing to the extreme permittivity value ($\varepsilon = 300 \times (1 + i10^{-3})$) of the ferroelectric cube used here, the magnetic and electric fields are highly concentrated within and in the

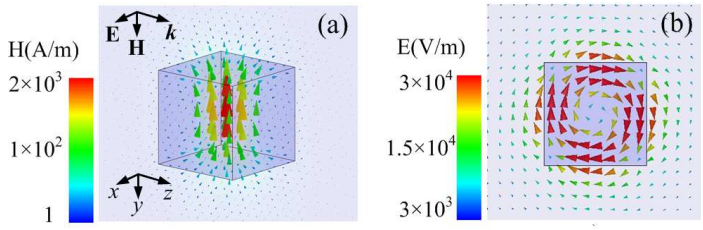

Figure 1. Field plots of a single STO cube ($a = 1.0\,\text{mm}$, $\varepsilon = 300 \times (1 + i10^{-3})$) at the 1st Mie resonance mode, $\omega_0 = 14.61\,\text{GHz}$. (a) Zoomed view of magnetic field vector, and (b) circular displacement currents induced by an external magnetic field (in the $y = 0$ plane).

vicinity of the cube. In other words, a single HPP stores the EM field which is subsequently re-radiated, at its resonance frequency and on a very small scale comparable with SSA dimension. This is the underlying idea of the present study which thus combines an ultra small loop-type antenna [25] via magnetic resonance effects and a sub-cutoff aperture for achieving enhanced transmission in a SSA system. Predictably, the transmission modifications are expected independent on polarization and incidence angle of the illumination thanks to the isotropic response of the high symmetry HPPs which will be considered in the present work [20, 22]. These properties are thus quite different from that originating from SRR's whose electromagnetic properties are highly anisotropic [15].

This paper is organized as follows: In Section 2, we present a numerical analysis (based on HFSS, a finite-element simulation code commercialized by Ansoft) of the enhanced transmission through a SSA in a copper plate under normal incidence by introducing a single HPP in close proximity. Special attention was paid to the effects of the real and imaginary parts of HPP permittivity and coupling distance on the overall transmission performance. Quasi-independent transmission enhancements on incidence angle of both TE and TM modes are reported in Section 3. Concluding remarks and prospects are reported in Section 4.

2. ENHANCED TRANSMISSION UNDER NORMAL INCIDENCE

Figure 2 shows the schematic of the transmission problem of concern, for which the transmission through a copper plate (with side length L and thickness $t = 30\,\mu\text{m}$) with a circular aperture (with a radius

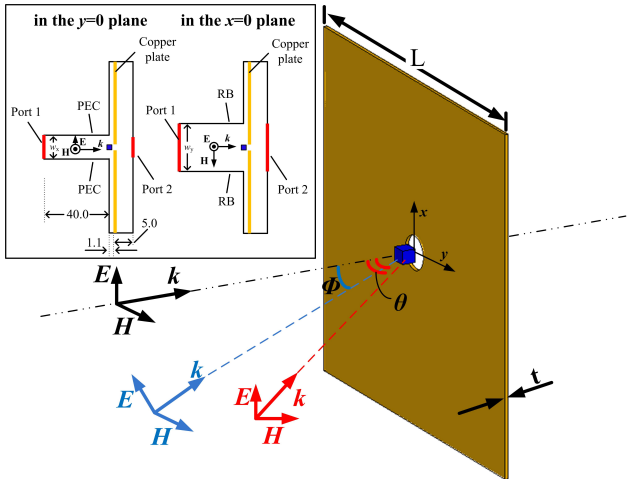

Figure 2. Schematic of the illumination of a single sub-wavelength aperture (SSA) in a metallic plate and a single High Permittivity Particle (HPP) with $d = 0.6\,\text{mm}$ away from the metal surface. Incidence plane of TM and TE mode is perpendicular to the y and x axis, respectively. Sectional views of simulation model in the $y = 0$ plane and $x = 0$ plane with dimensions of computational domain labeled in millimeter (mm) are shown in the inset.

R) is examined with and without the integration of a single HPP, respectively. Parallel to the copper plate, two ports whose dimensions were chosen according to the operating wavelength are used for excitation and detection. As shown in the insets of Fig. 2 with dimensions of computational domain labeled in millimeter (mm), by setting PEC (Perfect Electric Conductor) boundaries and "Radiation Boundaries (RB)" (for elimination of reflection) between excitation port (Port 1) and plate, we obtain a quasi-plane wave illumination with electric and magnetic fields oscillating along the x and y axis, respectively [22]. Other boundaries of the simulation model are set as RB to eliminate the multi-reflection. Furthermore, in order to investigate the sensitivity of the transmission enhancement to polarization and incidence angle, two fundamental operating TM and TE modes and, the corresponding incidence angle, ϕ and θ, were defined as those shown in Fig. 2, respectively.

It is known that the 1st Mie resonance of HPP is closely dependent on their bulk material parameter [16], i.e., permittivity $\varepsilon = \varepsilon_1(1 + i\tan\delta)$. Consequently, in our case, dielectric properties of the particle would then determine the modification of transmission through a SSA.

On the other hand, the distance from the center of HPP to the copper plate surface, which is defined as coupling distance d here (not labeled in Fig. 2 for clarity), would dominate the enhanced transmission as well. In order to clarify the dependence of the enhancement behavior on ε and d, transmissions through a SSA in the cases of placing a HPP with different ε_1, $\tan\delta$ and d are simulated under normal incidence and discussed in Subsection 2.1 and 2.2, respectively.

2.1. Dependence of Transmission Enhancement on ε_1

Figure 3 summarizes the results of this parametric analysis performed by varying ε_1 from 200 to 800 and by keeping $\tan\delta = 10^{-3}$. The frequency dependences of the transmission coefficient with and without HPP are plotted in solid and dashed lines respectively in Fig. 3(a), yielding the enhancement factor also reported in Figs. 3(b)–(e). The transmission spectra calculated for bare HPPs are displayed in the inset of Fig. 3(a). Notice that to reasonably characterize the 1st Mie resonance, in particular the resonance frequency of a single HPP, a unit cell with paired PEC and PMC (Perfect Magnetic Conductors) boundary conditions [20] is used to simulate plane-wave illuminating periodic array (one single layer in the direction of propagation) composed of HPPs. In addition, cubic lattice constant as large as $10a$ (where a is the cubic sidelength) has been assumed to eliminate coupling effect between different HPPs and approximate the behavior of a single particle. This is opposite to the attempt to manipulate EM wave through coupling effect between split ring resonators (SRRs) [26]. As seen in the insets of Fig. 3(a), the transmission spectra of bare HPPs ($a = 1.0\,\text{mm}$) exhibit a notch-like filtering characteristic at the 1st Mie resonance and we take the frequency of the dip as ω_0 of a single HPP. The resonance frequency shifts from the Ku band (12–18 GHz) to the X band (8–12 GHz) by increasing ε_1 from 200 to 800. Table 1 lists the parameters which have been used in the SSA transmission simulations. $\lambda_{0,\omega_0}/20$ (λ_{0,ω_0} is the operating wavelength) was chosen

Table 1. Material parameters and dimensions used in the simulations.

Cube ref. ($a = 1.0\,\text{mm}$)	ε_1	ω_0 (GHz)	R (mm)	L (mm)	$w_x \times w_y$ (mm^2)
# 1	200	17.82	0.83	50	4.32×10.67
# 2	400	12.62	1.20	70	19.05×9.52
# 3	600	10.31	1.50	90	22.86×10.16
# 4	800	8.93	1.67	100	22.86×10.16

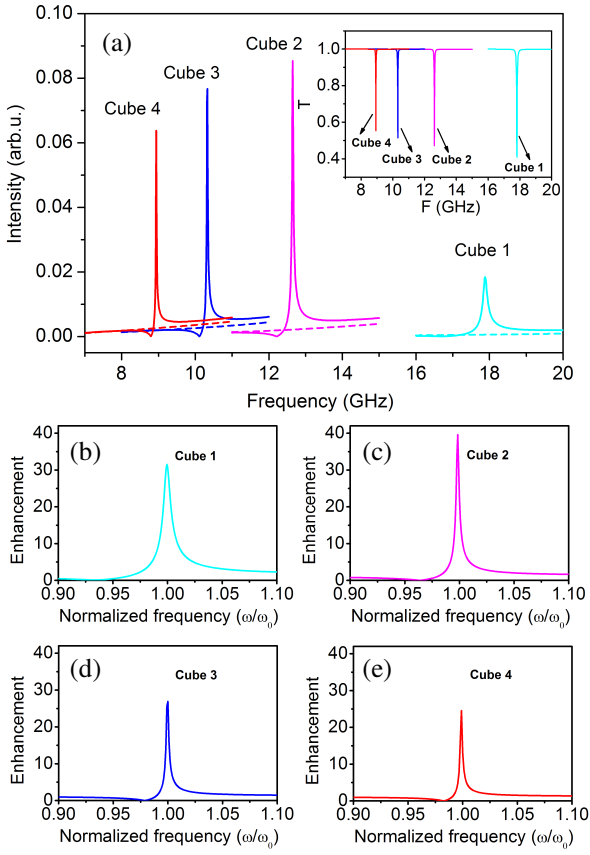

Figure 3. (a) Numerical results of transmitted wave intensity through a SSA without (dashed lines) and with a single HPP (solid lines) listed in Table 1. Corresponding transmission spectra of the HPP are shown in the insets. Dependence of enhancement versus the normalized frequency (ω/ω_0) corresponding to the 1st Mie resonance frequency ω_0 are shown in (b), (c), (d) and (e), respectively.

as a criterion of radius (R) of aperture and L is length of the copper plate. Notice that to validate the comparison of enhanced transmission of different cubes, we keep the ratio between the dimension of copper plate (i.e., L) and λ_{0,ω_0} as ~ 3. Dashed lines in Fig. 3(a) show the transmission spectra through SSA without HPP with a very weak transmission predicted by diffraction theory [2]. Solid lines indicate the corresponding transmission after placing a single HPP according to the schematics displayed in Fig. 2. Sharp transmission peak can be noticed

around the 1st Mie magnetic resonance mode ω_0 of various cubes, demonstrating a dramatic transmission enhancement through the SSA. Moreover, in order to compare the transmission enhancements as a function of the permittivity ε_1 listed in table, we plotted in Figs. 3(b), (c), (d) and (e) the ratio of the transmission with and without HPP, as a function of the normalized frequency ω/ω_0. We observed 32, 40, 27 and 24-fold maximum transmission enhancement in the presence of a single HPP with ε_1 of 200, 400, 600 and 800, respectively.

As discussed above, the transmission enhancement proposed here is primarily due to the HPP's EM energy concentration at ω_0. This energy concentration can be understood as follows, EM wave within the volume of $(\lambda_{0,\omega_0})^3$ is compressed into the space determined by the physical particle dimension (i.e., a here). In a first approximation, the resonance condition corresponding to ground eigenstate reads $k_1 a = \pi$, where $k_1 = 2\pi/\lambda_1$ is the wave vector in the material of particle. Taking only the magnetic polarization into account, which dominates the electromagnetic response at ω_0, the electric field of the magnetic dipole in the near field region ($kr \ll \lambda$) could be written as $\mathbf{E} = -ik(\mathbf{n}\times\mathbf{m})r^{-2}$, where $\mathbf{n}$ and $\mathbf{m}$ are unit vector along the direction from the center of magnetic dipole to detecting point and magnetic dipole moment [24]. If the spatial density of incident energy is constant, as it was assumed in the simulations, whatever the frequency band of interest, then the magnetic moment $\mathbf{m}$ of a particle (with certain dimension) increases with ε_1 owing to a stronger energy compression at lower operating frequency, while $k = 2\pi/(\lambda_{0,\omega_0})$ varies reversely. This could qualitatively interpret the fall-after-rising behavior of the maximum enhancement with the increasing ε_1, shown in Figs. 3(b)–(e).

The dielectric constant abovementioned can be achieved technologically by taking advantage of the developed ferroelectrics techniques. As an example in the following numerical studies, we take $SrTiO_3$ (STO) which has been widely accepted and applied as low loss microwave ferroelectrics. In other words, we use single crystal STO HHP with permittivity of $300 \times (1 + i10^{-3})$ [27, 28] and the corresponding $R = 1.0\,\text{mm}$ and $L = 60\,\text{mm}$ in the following simulations.

2.2. Effect of Dielectric Loss tan and Coupling Distance *d*

Besides ε_1, dielectric loss described by $\tan\delta$ is the other key factor for Mie resonance. Therefore, it can be seen from the inset of Fig. 4(a) that the notch depth at the 1st Mie resonance of STO particles degrades rapidly with increasing $\tan\delta$. This degradation, which is caused by the damping effect of the rotating displacement current (see Fig. 1(b)) implies weaker field concentration in/around the particle and inevitably plays an important role in the enhanced transmission

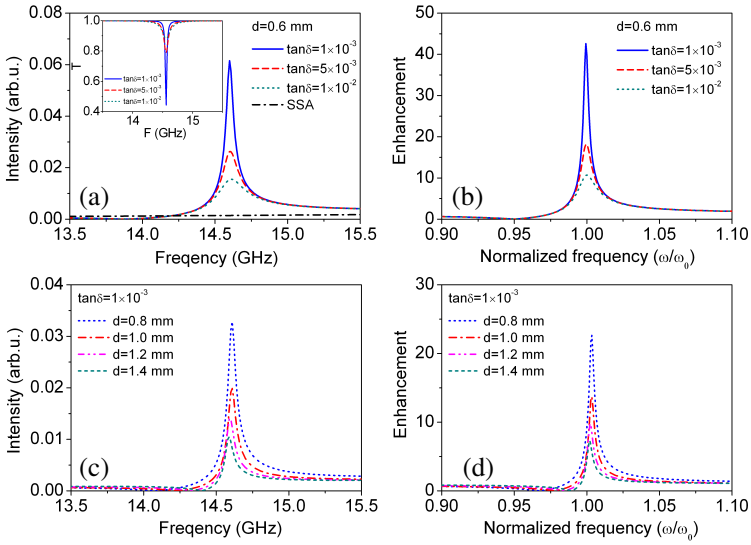

Figure 4. Effect of dielectric loss $\tan\delta$ (with $d = 0.6\,\text{mm}$): (a) Transmitted wave intensity through a SSA and that with a single STO cube ($\varepsilon_1 = 300$) with $\tan\delta = 10^{-3}$, 5×10^{-3} and 10^{-2}, respectively. Inset shows the transmission spectra of the corresponding STO cubes of various $\tan\delta$, and the corresponding. (b) Dependence of enhancement versus the normalized frequency (ω/ω_0). Effect of coupling distance d (STO cube with $\varepsilon_1 = 300$ and $\tan\delta = 10^{-3}$): (c) Transmitted wave intensity through a SSA with a single STO cube with coupling distance of $d = 0.8$, 1.0, 1.2 and 1.4mm, respectively, and the corresponding (d) Dependence of enhancement versus the normalized frequency.

through a SSA. Figs. 4(a) and (b) illustrates quantitatively the degradation effects by introducing STO cube ($a = 1.0\,\text{mm}$) with $\tan\delta = 10^{-3}$, 5×10^{-3} and 10^{-2}, respectively and by taking a constant value of $\varepsilon_1 = 300$ so that the transmission maximum is at the same frequency ω_0. Nevertheless, we can see that more than a 10-fold enhancement is expected to be achieved even when $\tan\delta$ is assumed 1%, which reveals a reasonable tolerance to dielectric loss of particle in this enhanced transmission phenomenon.

On the other hand, for the SSA system with certain HPP, the coupling distance d (from HPP center to copper plate surface) would dominate the enhancement behavior. Using STO cube with $a = 1.0\,\text{mm}$ and $\tan\delta = 10^{-3}$, Figs. 4(c) and (d) illustrate the decreasing maximum enhanced transmission with increasing d from

0.8 to 1.4 mm. It should be noted that the shape of the HPP particle distinctly controls its resonance and EM wave confinement, which would consequently plays a significant role in the enhanced transmission of the SSA system.

2.3. Field Distribution Illustration

To have further insight into the transmission modification by means of the HPP, time-snapshots of the electric field (E_x) recorded at 14.61 GHz are shown in Fig. 5, in which the left- and right- hand side figures correspond to a SSA without and with a STO cube, illuminated by a quasi-plane wave with the electric field perpendicular to the $x = 0$ plane (see Fig. 2). Figs. 5(a) and (c) illustrate the very weak intensity of the diffracted field through the SSA which hence results in a very low transmission level. In a first approximation the transmission level reduces roughly in the ratio $(R/\lambda_0)^4$, i.e., $(1/20)^4$ here theoretically [2]. In the presence of a STO cube, as shown in Figs. 5(b) and (d), the electric field magnitude behind the aperture increases dramatically with respect to the configuration without a cube. This accordingly

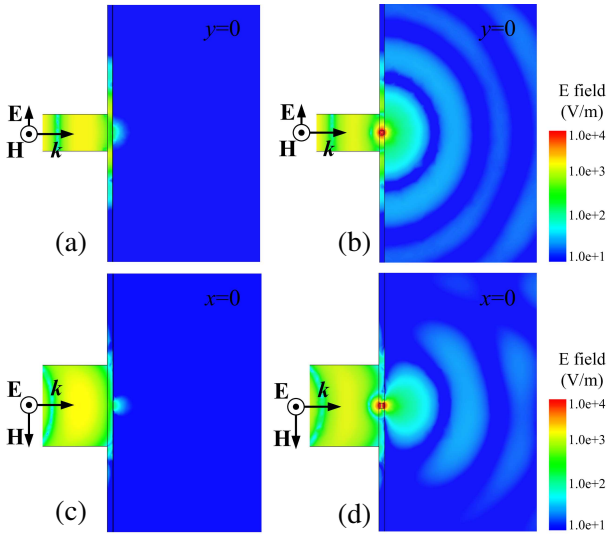

Figure 5. Time-snapshots of the electric field distribution Re(E_x) of a SSA setup in the $y = 0$ and $x = 0$ planes (see Fig. 2) are shown in (a) and (c), respectively. The corresponding electric field distribution Re(E_x) with a STO cube in the $y = 0$ and $x = 0$ planes (see Fig. 2) are shown in (b) and (d).

contributes to a high enhancement of transmission. On the other hand, the comparison between the field distributions reported in Figs. 5(b) and (d) in the vicinity of the aperture in the $y = 0$ and $x = 0$ planes (see Fig. 2), respectively, reveals an angular pattern which is dependent on the polarization of the incident radiation. This field distribution (behind the aperture) with circular symmetry in $y = 0$ plane and $\cos^2\theta$ variation in $x = 0$ plane coincides with that of a HPP's scattering at the 1st Mie resonance (as Fig. 1 shows), i.e., a half of the typical magnetic dipole emission pattern [24], which clearly illustrates the antenna-like performance of the HPP in the transmission enhancement through a SSA.

3. QUASI-INDEPENDENT ENHANCEMENT PROPERTIES TO INCIDENCE ANGLE UNDER TE AND TM MODES

As discussed above, transmission enhancement through a SSA is based upon the electromagnetic energy compression and re-radiation of the HPP at the 1st Mie resonance mode. On the other hand, very small dimensions comparable to aperture dimension, both being much shorter than the resonance wavelength (λ_{0,ω_0}), along with high geometrical symmetry are expected to be suitable for insensitivity to polarization and incidence angles in contrast to artificial metallic structures which are highly anisotropic. The fact that EM resonances of arrayed high permittivity particle are isotropic has been verified theoretically and experimentally [16–21]. Consequently, one could intuitively anticipate that the enhanced transmission investigated here would be highly independent on the illumination polarization and incidence angle. To verify this assumption, we examine in the following the transmission through a SSA by varying incidence angle under TM and TE modes, respectively.

3.1. Transmission Enhancement Under TM Mode

As indicated as the blue coordinate in Fig. 2, we define TM mode here as a tilted illumination with fixed magnetic field and incidence angle ϕ. Fig. 6 shows the figures of enhancement by means of a STO cube under various incidence angle ϕ, while the insets illustrate the corresponding transmission spectra. Together with distinct transmission peaks at the 1st Mie resonance frequency ($\omega_0 = 14.61\,\text{GHz}$) of the STO cube, a comparison of the various green curves in Fig. 6 reveals that the enhancement property could be preserved even with large incidence angle, though the absolute maximum of

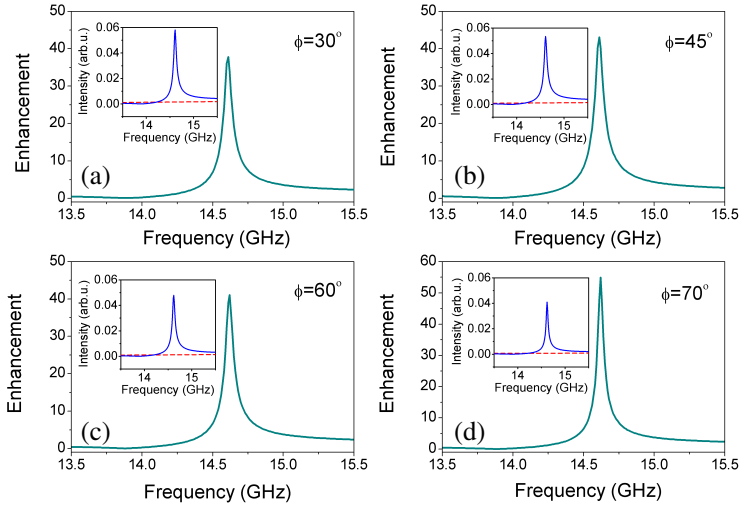

Figure 6. Quasi-independent transmission enhancement under TM mode. Frequency dependence of the enhancement ratio under different incidence angle ϕ of (a) 30°, (b) 45°, (c) 60° and (d) 70°. Corresponding transmission spectra of a SSA without (red dashed lines) and with a STO cube (blue solid lines) are shown in the insets, respectively.

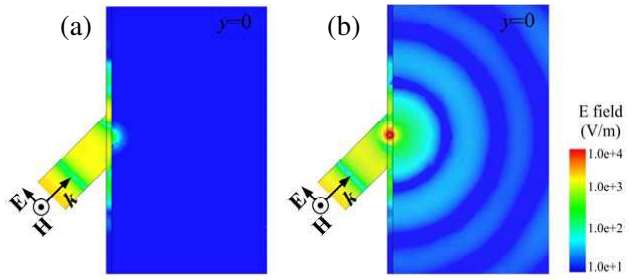

Figure 7. Time-snapshots of the electric field distribution Re(E_x) (at 14.61 GHz) of a SSA setup under TM mode in the plane of incidence (the $y = 0$ plane, see Fig. 2), (a) without and (b) with a STO cube for an incidence angle $\phi = 45°$.

transmission decreases gradually with increasing ϕ. Furthermore, the even larger enhancement (around 55-fold) in the case of $\phi = 70°$ distinctly indicates the almost independent transmission enhancement property under TM mode.

Figure 7 illustrates the time-snapshots of the electric field distribution Re(E_x) (at 14.61 GHz) of a SSA under TM mode in the

plane of incidence ($y = 0$ plane, see Fig. 2) without and with a STO cube, for an incidence angle $\phi = 45°$. Compared with (a) and (b) in Fig. 5, Fig. 7 clearly shows the enhanced field behind the aperture when placing a STO cube in front of it. The electric field distribution displays a typical magnetic dipole antenna radiation pattern.

3.2. Transmission Enhancement Under TE Mode

We define TE mode here as a tilted illumination (incidence angle θ) with fixed electric field, as shown in Fig. 2 as the red coordinate. Similar to Fig. 6, Fig. 8, with corresponding transmissions shown in the insets, indicates the enhancement in the presence of a STO cube under various incidence angle θ. Peaks, with close maximum value around 40-fold at the 1st Mie resonance frequency ($\omega_0 = 14.61\,\text{GHz}$) in the cases of different θ, show the quasi-independence of the enhancement property for TE mode. Comparison with Fig. 6 shows that for the same incidence angle (θ under TE mode and ϕ under TM mode) the maximum enhancements under the two modes are quite similar.

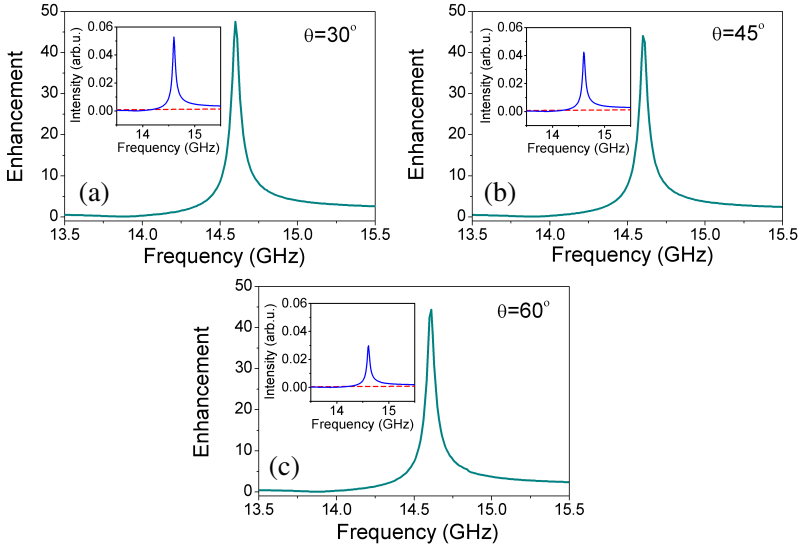

Figure 8. Quasi-independent transmission enhancement under TE mode. Dependence of enhancement on frequency under different incidence angle θ of 30°, 45° and 60° are shown in (a), (b) and (c), respectively. Corresponding transmission spectra of a SSA (red dashed lines) and that with a STO cube (blue solid lines) are shown in the insets.

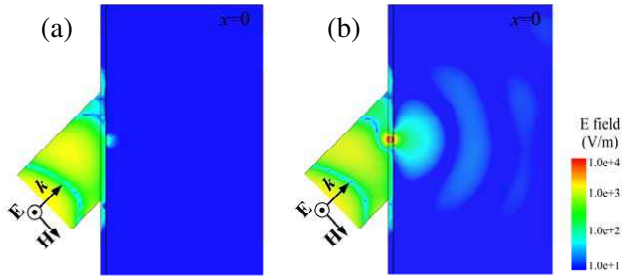

Figure 9. Time-snapshots of the electric field distribution Re(E_x) (at 14.61 GHz) of a SSA setup under TE mode in the plane of incidence (the $x = 0$ plane, see Fig. 2), (a)without and (b) with a STO cube for an incidence angle $\theta = 45°$.

Analogous to Fig. 7, with an incidence angle $\theta = 45°$, time-snapshots in the plane of incidence ($x = 0$ plane, see Fig. 2) of the electric field (Re(E_x)) at 14.61 GHz under TE mode are shown in Fig. 9. They demonstrate a strong radiation through a SSA arising from the STO cube resonance. In addition, the $\cos^2\theta$ dependent distribution pattern, which is comparable to that in Fig. 5(d), clearly reflects that radiation behind the aperture also follows that of the magnetic dipole antenna in the case of tilted illumination under TE mode.

4. CONCLUSION AND PROSPECTS

In summary, we numerically demonstrate that transmission through a single subwavelength aperture (SSA) system could be greatly enhanced by introducing a single high permittivity particle (HPP) operating at the 1st Mie resonance. This transmission enhancement originates from the electromagnetic energy compression and re-radiation of HPP at the Mie resonance frequency for which the HPP can be regarded as a magnetic dipole antenna. A parametric study shows that real part of permittivity of a ferroelectric $SrTiO_3$ cube used here as a HPP determines the central frequency of the enhanced transmission, while dielectric loss governs the maximum. Moreover, thanks to much smaller dimensions compared with operation wavelength and geometrical symmetry of the cube, we numerically show that enhanced transmission would be quasi-independent to both illumination polarization and incidence angle, which is distinct from the enhanced transmission afforded by split ring resonators [15]. Nevertheless, we also note that the capacity of enhancement we report in this paper is comparable to that of magnetically resonating SRR

(the D case in Ref. [15]), and below those of electrically resonating ones (the A and B cases in Ref. [15]), which intrinsically originates from the lower radiation efficiency of magnetic dipole [24]. The transmission enhancement through a SSA system, demonstrated here numerically, is predictably tunable, due to the dielectric constant sensitivity of ferroelectrics notably on temperature, electric field and so on [29–31] and to corresponding controllable Mie resonance of HPP [32]. It should be also noted that, strong Mie resonance has also been verified experimentally at THz [21] and midinfrared frequencies [18] in STO and SiC particles, respectively. And in consequence, the functioning frequency of transmission enhancement proposed here could be utilized in a broad frequency range.

ACKNOWLEDGMENT

Lei Kang has been supported by Erasmus Mundus External Cooperation Window LiSUM project.

REFERENCES

1. Genet, C. and T. W. Ebbesen, "Light in tiny holes," *Nature*, Vol. 445, 39–46, 2007.
2. Bethe, H. A., "Theory of diffraction by small holes," *Phys. Rev.*, Vol. 66, 163–182, 1944.
3. Garcia-Vidal, F. J., E. Moreno, J. A. Porto, and L. Martin-Moreno, "Transmission of light through a single rectangular hole," *Phys. Rev. Lett.*, Vol. 95, 103901, 2005.
4. Chang, C. W., A. K. Sarychev, and V. M. Shalaev, "Light diffraction by a subwavelength circular aperture," *Laser Phys. Lett.*, Vol. 2, 351–355, 2005.
5. Popov, E., N. Bonod, M. Nevière, H. Rigneault, P.-F. Lenne, and P. Chaumet, "Surface plasmon excitation on a single subwavelength hole in a metallic sheet," *Appl. Opt.*, Vol. 44, 2332–2337, 2005.
6. Webb, K. J. and J. Li, "Analysis of transmission through small apertures in conducting films," *Phys. Rev. B*, Vol. 73, 033401, 2006.
7. Garcia de Abajo, F., "Light transmission through a single cylindrical hole in a metallic film," *Opt. Express*, Vol. 10, 1475–1484, 2002.
8. Popov, E., M. Nevière, A. Sentenac, N. Bonod, A.-L. Fehrembach, J. Wenger, P.-F. Lenne, and H. Rigneault, "Single-scattering

theory of light diffraction by a circular subwavelength aperture in a finitely conducting screen," *J. Opt. Soc. Am. A*, Vol. 24, 339–358, 2007.

9. Michalski, K. A., "Complex image method analysis of a plane wave-excited subwavelength circular aperture in a planar screen," *Progress In Electromagnetics Research B*, Vol. 27, 253–272, 2011.
10. Obermüller, C. and K. Karrai, "Far-field characterization of diffracting apertures," *Appl. Phys. Lett.*, Vol. 67, 3408–3410, 1995.
11. Degiron, A., H. J. Lezec, N. Yamamoto, and T. W. Ebbesen, "Optical transmission properties of a single subwavelength aperture in a real metal," *Opt. Commun.*, Vol. 239, 61–66, 2004.
12. Yin, L., V. K. Vlasko-Vlasov, A. Rydh, J. Pearson, U. Welp, S.-H. Chang, S. K. Gray, G. C. Schatz, D. B. Brown, and C. W. Kimball, "Surface palsmons at single nanoholes in Au films," *Appl. Phys. Lett.*, Vol. 85, 467–469, 2004.
13. Lezec, H. J., A. Degiron, E. Devaux, R. A. Linke, L. Martin-Moreno, F. J. Garcia-Vidal, and T. W. Ebbesen, "Beaming light from a subwavelength aperture," *Science*, Vol. 297, 820–822, 2002.
14. Akarca-Biyikli, S. S., I. Bulu, and E. Ozbay, "Enhanced transmission of microwave radiation in one-dimensional metallic gratings with subwavelength aperture," *Appl. Phys. Lett.*, Vol. 85, 1098–1100, 2004.
15. Aydin, K., A. O. Cakmak, L. Sahin, Z. Li, F. Bilotti, L. Vegni, and E. Ozbay, "Split-ring-resonator-coupled enhanced transmission through a single subwavelength aperture," *Phys. Rev. Lett.*, Vol. 102, 013904, 2009.
16. Pendry, J. B., A. J. Holden, D. J. Robbins, and W. J. Stewart, "Magnetism from conductors and enhanced nonlinear phenomena," *IEEE Trans. Microwave Theory Techn.*, Vol. 47, 2075–2084, 1999.
17. Holloway, C. L., E. F. Kuester, J. Baker-Jarvis, and P. Kabos, "A double negative (DNG) composite medium composed of magnetodielectric spherical particles embedded in a matrix," *IEEE Trans. Antennas Propag.*, Vol. 51, 2596–2603, 2003.
18. Schuller, J. A., R. Zia, T. Taubner, and M. L. Brongersma, "Dielectric metamaterials based on electric and magnetic resonances of silicon carbide particles," *Phys. Rev. Lett.*, Vol. 99, 107401, 2007.
19. Popa, B. and S. A. Cummer, "Compact dielectric particles as a building block for low-loss magnetic metamaterials," *Phys. Rev. Lett.*, Vol. 100, 207401, 2008.

20. Zhao, Q., L. Kang, B. Du, H. Zhao, Q. Xie, X. Huang, B. Li, J. Zhou, and L. Li, "Experimental demonstration of isotropic negative permeability in a three-dimensional dielectric composite," *Phys. Rev. Lett.*, Vol. 101, 027402, 2008.
21. Nemec, H., P. Kuzel, F. Kadlec, C. Kadlec, R. Yahiaoui, and P. Mounaix, "Tunable terahertz metamaterials with negative permeability," *Phys. Rev. B*, Vol. 79, 241108(R), 2009.
22. Zhang, F., Q. Zhao, L. Kang, J. Zhou, and D. Lippens, "Experimental verification of isotropic and polarization properties of high permittivity-based metamaterial," *Phys. Rev. B*, Vol. 80, 195119, 2009.
23. Zhao, Q., J. Zhou, F. Zhang, and D. Lippens, "Mie resonance based dielectric metamaterial," *Materials Today*, Vol. 12, 60, 2009.
24. Jackson, J. D., *Classical Electrodynamics*, Wiley, New York, 1999.
25. Balanis, C., *Antenna Theory, Analysis, and Design*, 2nd Edition, Wiley, New York, 1997.
26. Carbonell, J., E. Lheurette, and D. Lippens, "From rejection to transmission with stacked arrays of split ring resonators," *Progress In Electromagnetics Research*, Vol. 112, 215–224, 2011.
27. Vendik, O. G., L. T. Ter-Martirosyan, and S. P. Zubko, "Microwave losses in incipient ferroelectrics as functions of the temperature and the biasing field," *J. Appl. Phys.*, Vol. 84, 993–998, 1998.
28. Geyer, R. G., B. Riddle, J. Krupka, and L. A. Boatner, "Microwave dielectric properties of single-crystal quantum paraelectrics $KTaO_3$ and $SrTiO_3$ at cryogenic temperatures," *J. Appl. Phys.*, Vol. 97, 104111, 2005.
29. Vendik, O. G. and S. P. Zubko, "Modeling the dielectric response of incipient ferroelectrics," *J. Appl. Phys.*, Vol. 82, 4475–4483, 1997.
30. Shaw, T. M., Z. Suo, M. Huang, E. Liniger, R. B. Laibowitz, and J. D. Baniecki, "The effect of stress on the dielectric properties of barium strontium titanate thin films," *Appl. Phys. Lett.*, Vol. 75, 2129–2131, 1999.
31. Molla, J., M. Gonzalez, R. Vila, and A. Ibarra, "Effect of humidity on microwave dielectric losses of porous alumina," *J. Appl. Phys.*, Vol. 85, 1727–1730, 1999.
32. Zhao, Q., B. Du, L. Kang, H. Zhao, Q. Xie, B. Li, X. Zhang, J. Zhou, L. Li, and Y. Meng, "Tunable negative permeability in an isotropic dielectric composite," *Appl. Phys. Lett.*, Vol. 92, 051106, 2008.